

## THE HIDDEN BEAUTY OF GOLD

Eckhard Hitzer and Christian Perwass\*

Department of Applied Physics, Fukui University, Fukui 910-8507, Japan

\* Department of Computer Science, Christian-Albrechts-University Kiel, Kiel 24103, Germany

### ABSTRACT

This paper first reviews the history, the economy, the material properties, and the applications of gold. Then the geometry of the fcc gold lattice is introduced. Based on the symmetric arrangement of atoms the gold lattice has a rich variety of symmetry transformations, that interchange the positions of atoms, but leave the lattice as a whole invariant. This begins with the point group symmetry of a single fcc lattice cell and is extended by combination with lattice translations to the full space group symmetry of the whole (practically infinite) lattice. We use the newly created interactive Space Group Visualizer (based on geometric algebra) in order to systematically picture all these symmetries. We can thus understand their origin and their relationships. In particular we give a full geometric explanation of the 192 screw symmetries passing through a single fcc cell of the gold lattice.

### 1. INTRODUCTION

What is *gold*? It is a metal that occurs as nuggets or grains in rocks, underground *veins* and in alluvial (river) deposits. Gold is dense (19.3 tons/m<sup>3</sup>), soft, shiny and the most malleable and ductile of the known metals. Pure gold has an attractive bright yellow color.

Gold has a rich history. It is mentioned 430 times in the Bible. First in Genesis a river around the Garden of Eden is described as “it winds through the entire land of Havilah, where there is *gold*.” (Gen. 2:11). When Jesus was born, three magi (wise men) followed a star and visited him. Their presents were: “gifts of *gold* and of incense and of myrrh.” (Mat. 2:11). The last book of the Bible describes the heavenly Jerusalem with “The great street of the city was of *pure gold*, like transparent glass.” (Rev. 21:21).

It has been estimated that all the gold in the world that has ever been refined would form a single cube of 20m on a side. Economic gold extraction starts with as little as 0.5g/1000kg ore. The deepest gold mines in South Africa, the Savuka and TauTona mines reach 3777m depth. Only 3 parts per billion of the Earth’s crust is gold, making it very rare. The world’s oceans hold vast amounts of gold in very low concentration of ca. 0.1 parts per billion. The largest gold depository is in the US Federal Reserve Bank in New York, with about 3% of all the gold ever mined. On October 1, 2007, the

gold price stood high at \$743.70 per ounce (31.1g).

Modern industrial uses include dentistry and electronics, because of its good conductivity and good resistance to oxidative corrosion [8]. Gold has been used in some high energy applications. It is also used in the connectors of more expensive electronic cables, such as audio, video and USB cables. Gold is further used for electronic sliding contacts in highly humid or corrosive atmospheres, and in contacts with very high failure cost (certain computers, communication equipment, spacecraft, jet air engines).

Gold is a good reflector of infrared and visible light. It is used for protective coatings on satellites, infrared protective faceplates, thermal protection suits and astronaut helmets. Automobiles like the McLaren F1 use gold foil in the engine compartment for heat insulation.

*Colloidal gold* (sols of gold nanoparticles) in water are intensely red-colored, used in research applications in medicine, biology and material science. Colloidal gold is also present in gold paint on ceramics prior to firing.

Gold can be drawn into very thin wires. A single gram of gold can be beaten into a *gold leaf* sheet of one square meter. Gold leaf can be beaten thin enough to become translucent (light shining through). The transmitted light appears greenish blue, because gold strongly reflects yellow and red. Native gold contains usually eight to ten percent silver. Gold readily forms alloys with

many other metals. These alloys can increase the hardness or produce exotic colors. The Japanese Mokume-gane craft exploits color contrasts between laminated gold alloys to produce wood-grain effects.

The gold content of alloys is measured in carats (k), with pure gold having 24k. *Blue gold* can be made by alloying with iron and *purple gold* can be made with aluminium. 14k and 18k gold alloys with silver alone appear greenish-yellow and are referred to as *green gold*. In photography gold toners are used.

The Canadian *Gold Maple Leaf* coin contains the highest purity gold of 99.999%. In 2007 the Canadian Mint produced a 100 kg gold coin with a face value of \$1 million, the gold content being worth over \$2 million. It measures 50 cm in diameter and is 3 cm thick. Wedding rings are traditionally made of gold.

Chemically it is a univalent and trivalent transition metal with 79 protons (and electrons), 118 neutrons (stable isotope) and the symbol **Au** (from Latin aurum). Gold does not react with most chemicals, but is attacked by chlorine, fluorine, aqua regia and cyanide. Gold dissolves in mercury, forming amalgam alloys, but does not react with it. Gold is insoluble in nitric acid, which will dissolve silver and other base metals, and this is the basis of the gold refining technique *inquartation and parting*.

The physical properties of gold are: A melting point of 1064.18 C, a heat capacity of 25.418 J/mol/K, thermal conductivity of 318 W/m/K, thermal expansion of  $14.2 \cdot 10^{-6}$  m/m/K, Young's modulus of 78 GPa, shear modulus of 27 GPa, bulk modulus of 220 GPa, Poisson ratio 0.44, Mohs hardness 2.5, Vickers hardness 216 MPa, and a Brinell hardness of 2450 MPa.

Gold solder is used for joining the components of gold jewellery by high-temperature hard soldering or brazing. Gold solder is usually made in at least three melting point ranges referred to as Easy, Medium and Hard. By using hard first, followed by the solders with progressively lower melting points, goldsmiths can assemble complex items with several separate soldered joints.

Gold alloys are used in restorative dentistry, for crowns and permanent bridges. The gold alloy's slight malleability facilitates the creation of a superior molar mating surface with other teeth, more satisfactory than surfaces produced by porcelain crowns.

Goldwasser (German for *Goldwater*) is a traditional liqueur produced in Gdansk (Poland)

and Schwabach (Germany), it contains flakes of gold leaf. [8]

## 2. THE GEOMETRY OF GOLD

*Geometrically* gold atoms are arranged in a cubic face centered (fcc) structure similar to the one shown in Fig. 1, also called cubic close packed (ccp). The edge lengths of this elementary cell cube is  $|a| = 407.82$  pm ( $1 \text{ pm} = 10^{-12} \text{ m}$ ) and the cube corner to face center distance  $|b|/2 = 288.4$  pm [16]. The atomic radius is 135 pm. Other elements with this structure are Al, Cu, Ni, Sr, Rh, Pd, Ag, Ce, Tb, Ir, Pt, Pb, and Th.

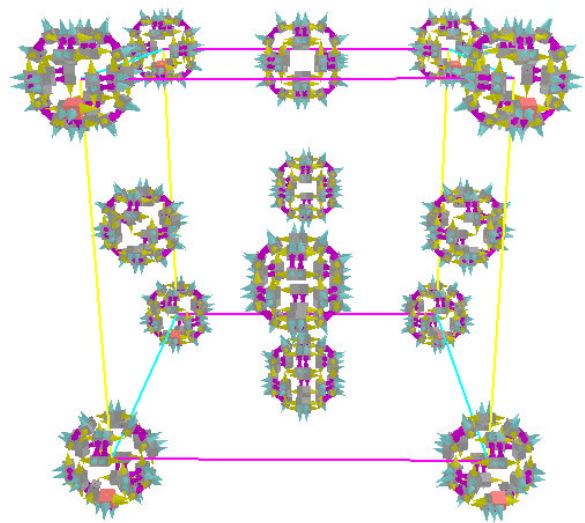


Fig. 1 A cubic face centered cell as seen in the Space Group Visualizer Demo 2.0 [7].

A fcc cell lattice is highly symmetric. That means there is an enormous variety of possible geometric transformations, that leave the lattice as a whole invariant, including all lengths and angles.

These symmetry operations include single cell transformations that leave a cell vertex *point invariant*: planes of *reflections* (through the vertex), *rotations* (with axis through the vertex), and *inversions* ( $x \rightarrow -x$ , relative to the vertex), and *rotoinversions* (inversions followed by a rotation, equivalent to rotations followed by a reflection at the rotation plane). This group of symmetries of a cell is called its *point group* [3,10,11] and serves for the classification of crystals, therefore it is also called *crystal class* [2].

The 48 symmetry transformations of the full cubic point group create 48 symmetric copies of

a general asymmetric element placed next to the invariant point. These small 48 element clusters appear in Fig. 1 around each fcc lattice vertex. An enlargement is shown in Fig. 2. In pure gold one atom is located at the center of this cluster.

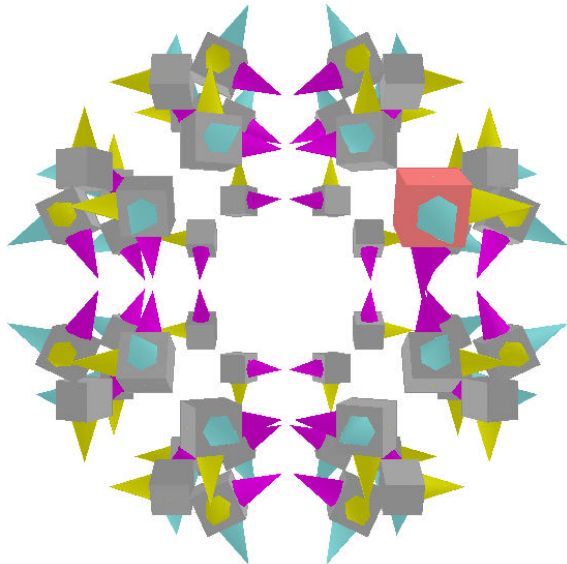


Fig. 2 48 general elements in 3D corresponding to the full cubic point symmetry.

The inclusion of integer lattice translations (from vertex to vertex) can lead to new planes of reflection. All possible planes of reflection passing through a single fcc cell are shown in Fig. 3.

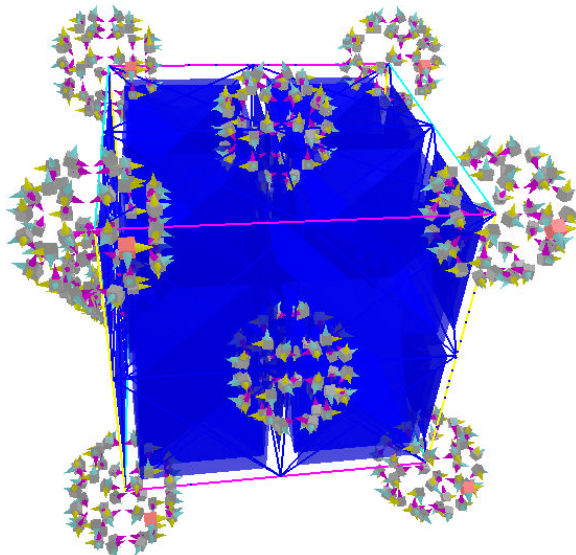


Fig. 3 All reflection planes of the fcc lattice passing through a single lattice cell.

The combination of a plane of reflection with a lattice translation not perpendicular to the plane leads to a combined *glide reflection*. The perpendicular translation component displaces the reflection plane in normal direction, and the parallel translation component creates a glide motion parallel to the plane. The set of all such glide planes passing through a single fcc cell is depicted in Fig. 4. The (red) vectors indicate the parallel glide motion.

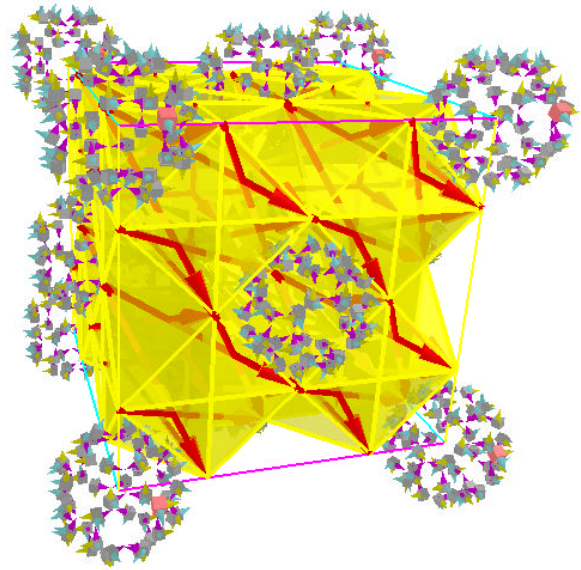


Fig. 4 All glide planes of the fcc lattice passing through a single lattice cell.

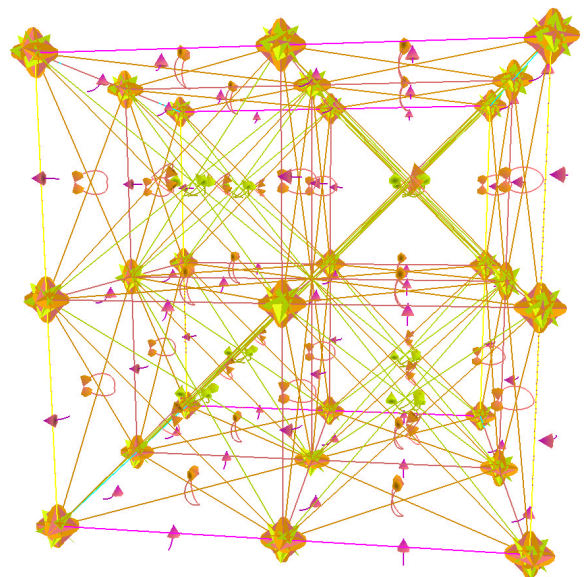


Fig. 5 All symmetry rotation axis passing through a single fcc lattice cell. Angles are indicated by colors and arc segments.

A sequence of two reflections at two planes results in a *rotation*. This rotation has the intersection line of the two planes as its axis and twice the (dihedral) angle between the two planes is the resulting rotation angle. All symmetry rotations of an fcc lattice cell arise in this way, they are depicted in Fig. 5. The relation between Fig. 3 of all reflection planes and Fig. 5 is that all the rotation axis seen in Fig. 5 are lines of intersection of reflection planes of Fig. 3.

If we perform a lattice translation perpendicular to the rotation axis after a rotation, we effectively create another rotation also already contained in Fig. 5. But if we perform a translation not normal to the rotation axis, with a translation component parallel to the rotation axis, we get a new transformation, a so-called *screw*. Provided that the parallel component itself is shorter as any lattice vector connecting any two vertexes. So a screw is a rotation followed by a translation along the screw axis, resulting in a directed helical motion around the screw axis. All (color coded) screws passing through a single fcc lattice are shown in Fig. 6. There are many more screws than rotations, because different translations (not normal to the rotation axis) of the same rotation lead to different screws.

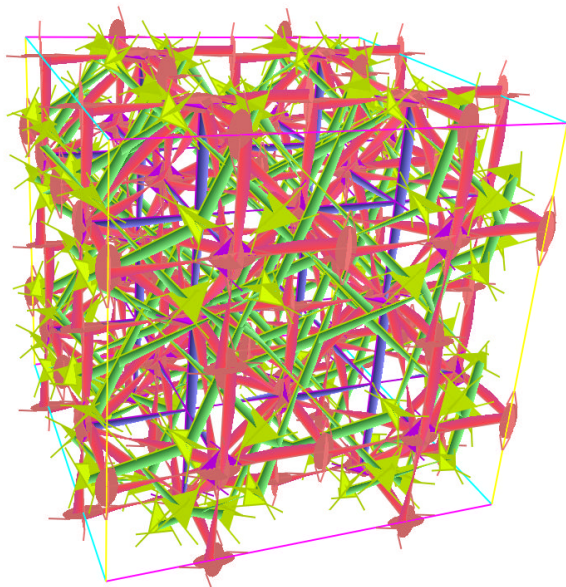


Fig. 6 All screw symmetry axis passing through a single fcc lattice cell.

Combining an inversion with a subsequent lattice translation yields a new center of inversion. All centers of inversion in a single fcc

lattice cell are depicted in Fig. 7.

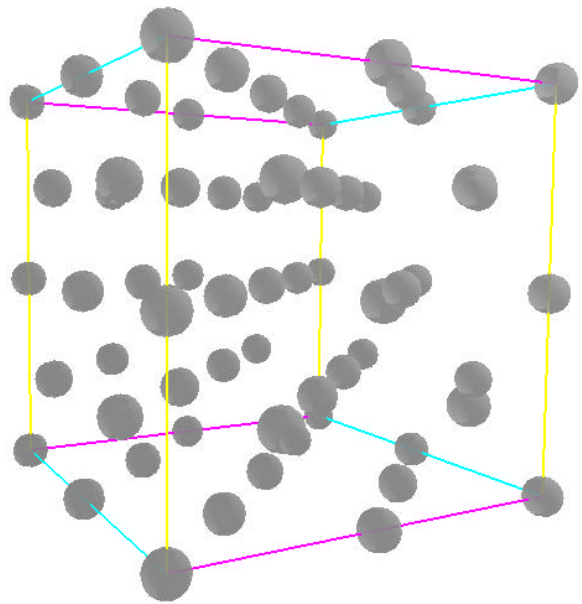


Fig. 7 All centers of inversion located in a single cell of a fcc lattice.

The combination of an inversion with a rotation leads to a *rotoinversion*. Characteristic for the fcc lattice are the 90 degree rotoinversions depicted in Fig. 8.

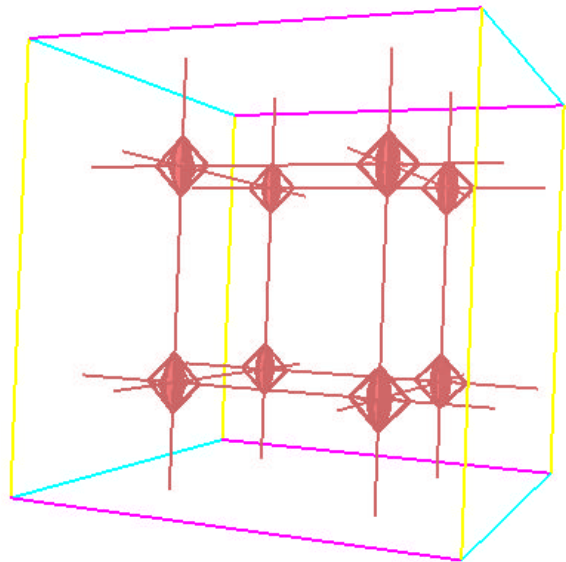


Fig. 8 All rotoinversions passing through a single fcc lattice cell.

The total graphical depiction of these symmetries in Fig. 9 gives an idea of the intricate complexity of the symmetries possessed

by the fcc lattice.

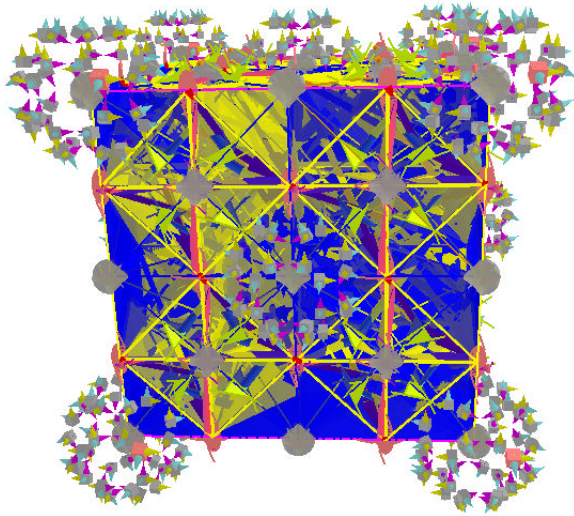


Fig. 9 Total depiction of all symmetries located in a single fcc cell.

The International Tables of Crystallography [2] depict the symmetries of a fcc cell by showing a quarter of an orthographic 2D projection of a side of a cube like in Fig. 10.

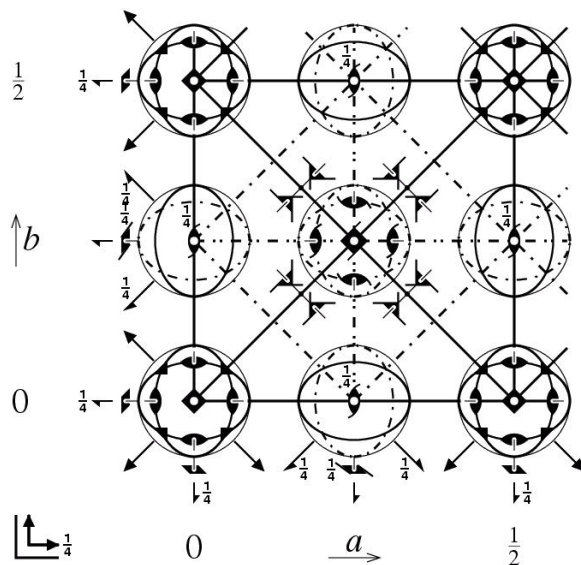


Fig. 10 Depiction [19] of the symmetries of an fcc lattice cell like in the International Tables of Crystallography [2], showing the orthographic projection of a lower left quarter of a side face.

Only a well-initiated expert can understand how the symmetries of Figs. 3 to 9 are all encoded in Fig. 10. Fig. 6 has shown the particular abundance of screws in fcc cells. We will have a

detailed look at these screw symmetries in the rest of this paper.

### 3. SCREWS IN FCC CELLS

We will not take a formal coordinate system and matrix approach [2]. Instead we first employ the Space Group Visualizer [4,5,7,11-15] to literally see what screws are present and then try to understand [1] their relationship to the rotations of Fig. 5.

#### 3.1 Pictorial Atlas of Gold Screws

We now image all screws present in a single fcc gold lattice cell beginning with right angle ( $90^\circ$ ) screws, continuing with the more frequent  $180^\circ$  screws, and culminating in the very abundant  $120^\circ$  screws. We use the SGV [7] based on CLUCalc [6].

##### 3.1.1 Screws of $90^\circ$

The fcc lattice has altogether 12 screws of  $90^\circ$  with screw index  $4_2$ . That means turning the screw two times by  $90^\circ$  will lead to a full lattice translation in the direction of the screw axis, i.e. turning once by  $90^\circ$  leads to half a lattice translation in axis direction. Always four screw axis are parallel to one cube edge, located in distances of  $1/4$  along face diagonals from the center of the face in all four directions (Fig. 11).

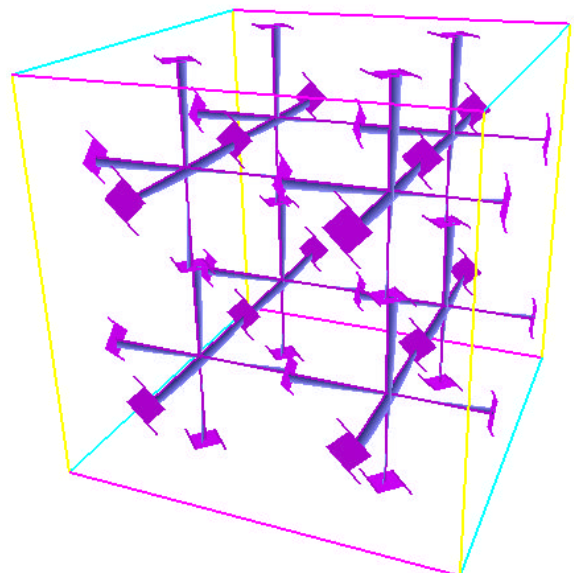


Fig. 11 Complete set of all twelve  $90^\circ$ -screws (symbol  $4_2$ ) passing through a single fcc lattice cell.

### 3.1.2 Screws of 180°

All 180°-screws (symbol  $2_1$ ) of a single fcc lattice cell are shown in Fig. 12. Repeating the screw motion two times gives a full 360° rotation combined with a full lattice translation. Obviously there are too many to easily count them.

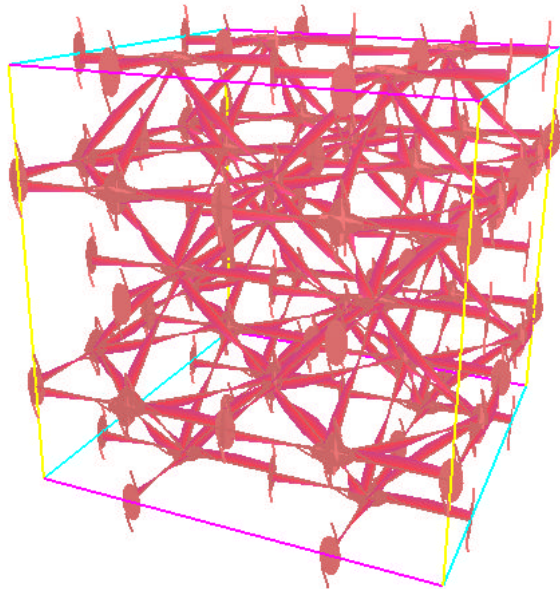


Fig. 12 All 180°-screws (symbol  $2_1$ ) passing through a single fcc lattice cell.

We therefore count how many screws are parallel to one edge, which is 12 according to Fig. 13. Times three we get 36 180°-screws parallel to all three edges. We further count how many screws are parallel to one face diagonal and find eight (Fig. 14). There are 6 face diagonals, so we get a total of  $6 \cdot 8 = 48$  180°-screws parallel to face diagonals. Hence there are  $36 + 48 = 84$  180°-screws in total.

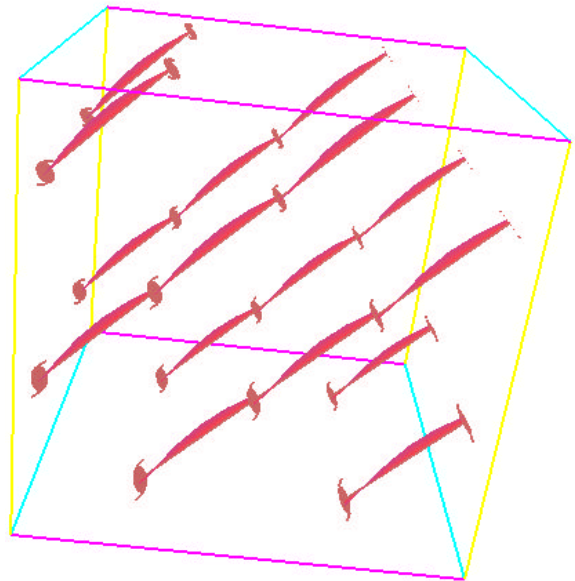


Fig. 14 All eight 180°-screws parallel to one face diagonal contained in a single fcc lattice cell.

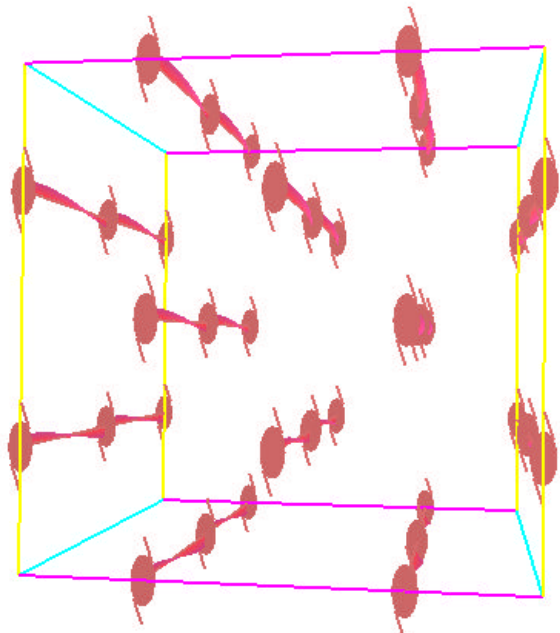


Fig. 13 All twelve 180°-screws parallel to one edge contained in a single fcc lattice cell.

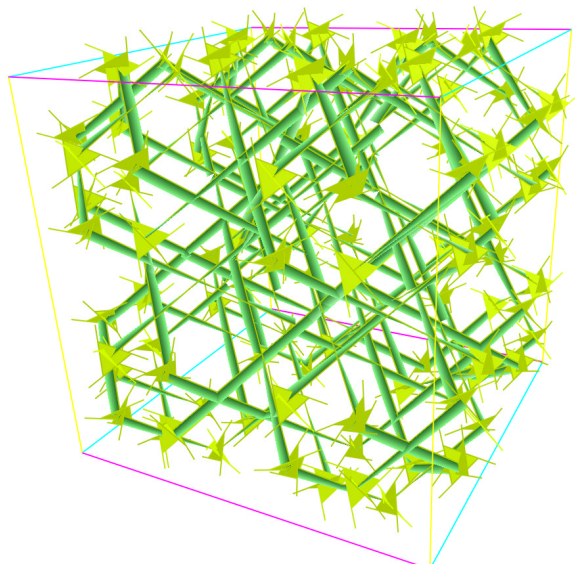


Fig. 15 All 120°-screws passing through a single fcc lattice cell.

### 3.1.3 Screws of 120°

All 120°-screws of a single fcc lattice cell are shown in Fig. 15. How many are there? Do they all have the same rotation angles and the same translation distance (albeit in different directions)? A close look at Fig. 15 shows that all 120°-screws are parallel to one of the 4 space diagonals. Exactly what we expect, because only the rotations around the space diagonals are 120° rotations. And combinations of these rotations with translations must lead to the 120°-screws. But even blending out three of the space diagonal directions (Fig. 16) makes the counting not without ambiguity.

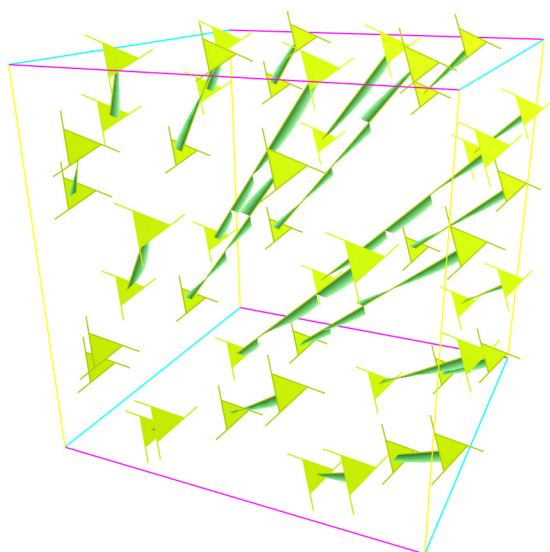


Fig. 16 All 120°-screws parallel to one space diagonal passing through a single fcc lattice cell.

We therefore employ the orthographic view along one of the space diagonals and now we can easily count that there are 12 screws of one type and 12 screws of another type. Experimenting with the interactive animation we see that in the visualization all screws turn in the same direction by 120°, but the translation motion by 1/3 along the space diagonal is in two opposite directions. One kind of screw has the symbol  $3_1$ , the other  $3_2$ . Screws related in this way are called *enantiomorphic*.

So we have  $12+12=24$  120°-screws parallel to one space diagonal. This leads to a total of  $4 \cdot 24 = 96$  120°-screws passing through a single fcc cell. Only four short of hundred, and a dozen more than the 84 180°-screws.

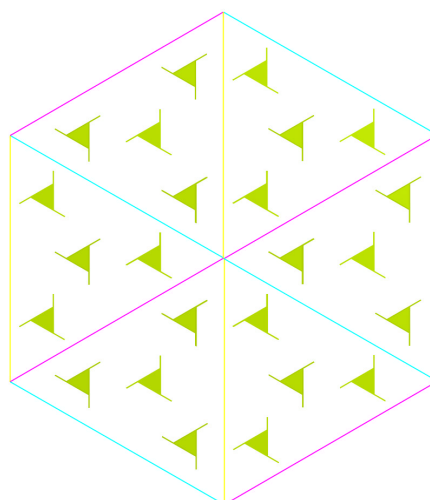


Fig. 17 Orthographic view along one space diagonal of all 120°-screws parallel to this space diagonal, passing through a single fcc lattice cell.

After we know what and how many screws there are, we only need to understand where they come from, i.e. how do point group rotations and lattice translations together produce this abundance of  $12 + 84 + 96 = 192$  screws of all angles and orientations?

### 3.2 The Origin of Screws

Now we investigate where the 192 screws passing through a single fcc cell come from.

#### 3.2.1 Combining Rotations and Translations

When a rotation  $R$  is followed by a translation  $T(t)$ , with the translation vector  $t$  in the plane of the rotation, we will get a shift  $T(s)$  of the rotation axis in the plane of the rotation, depending on the rotation angle. The resulting rotation  $R' = RT(t)$  can be described in terms of the old rotation  $R$  by *back translation* to the old axis with  $T(-s)$ , applying  $R$ , and *forward translation* again with  $T(s)$  to the new axis. So we have

$$R' = R T(t) = T(-s) R T(s) . \quad (1)$$

The question is now, how can we calculate the shift vector  $s$  in the plane of rotation? We can apply a  $T(-s)$  translation to (1) from the right and get

$$R T(t) T(-s) = T(-s) R T(s) T(-s) . \quad (2)$$

Combining the translations gives

$$R T(t-s) = T(-s) R . \quad (3)$$

Applying an inverse rotation  $R^{-1}$  from the left we get the translator identity

$$T(t-s) = R^{-1} T(-s) R = T(-R^{-1}s R) . \quad (4)$$

So we end up with the translation vector relationship

$$t-s = -R^{-1}s R . \quad (5)$$

Equation (5) is solved in the appendix and gives

$$s = ( t + \cot(\theta/2) t' )/2 , \quad (6)$$

where  $t'$  is obtained by rotating  $t$  anticlockwise by  $90^\circ$  in the plane of the rotation  $R$ . Table 1 lists the resulting axis shifts  $s$  for the fcc rotation angles  $\theta = 90^\circ, -90^\circ, 120^\circ, -120^\circ,$  and  $180^\circ$ , and Fig. 18 illustrates the situation for  $\theta = 90^\circ, 120^\circ,$  and  $180^\circ$ , the rotation centers  $s$  for  $\theta = -90^\circ, -120^\circ$  have the same horizontal component, but opposite vertical component.

Table 1 Rotation axis shifts  $s$ , due to combination of rotation  $R(\theta)$  with lattice translation  $t$  (in the plane of  $R$ ).

$\theta$	$\cot(\theta/2)$	$s$
$90^\circ$	1	$(t+t')/2$
$-90^\circ$	-1	$(t-t')/2$
$120^\circ$	$1/\sqrt{3}$	$(t + t'/\sqrt{3})/2$
$-120^\circ$	$-1/\sqrt{3}$	$(t - t'/\sqrt{3})/2$
$180^\circ$	0	$t/2$

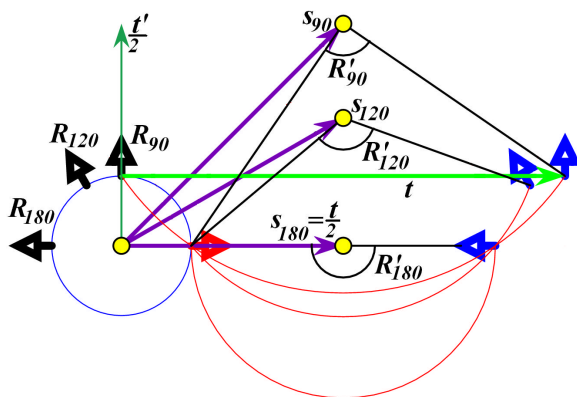


Fig. 18 Combinations of rotations  $R_\theta$  and translations  $T(t)$  result in shifted rotation centers  $s_\theta$ . Rotation axis vertical to paper plane, translations in paper plane.

We have dealt with translations in the plane of the rotation. Translations perpendicular to the plane of rotation (parallel to the rotation axis) simply change the rotation into a screw, without dislocating the axis.

### 3.2.2 Explaining $90^\circ$ Screws

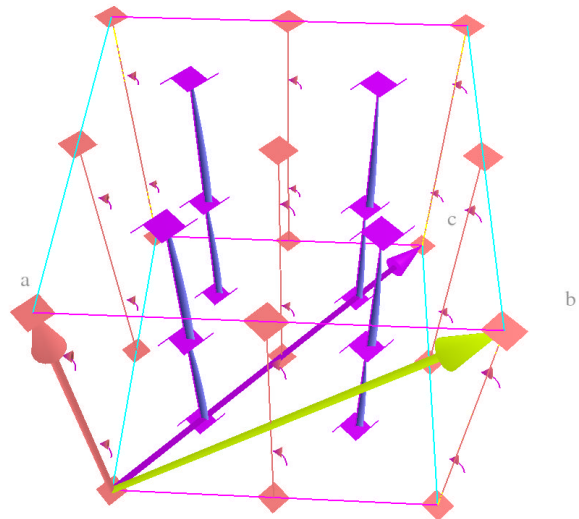


Fig. 19 All nine  $90^\circ$  rotations and all four screws parallel to lattice vector  $a$ ,  $c$  face diagonal perpendicular to  $a$ ,  $b$  face diagonal at  $45^\circ$  with  $a$ .

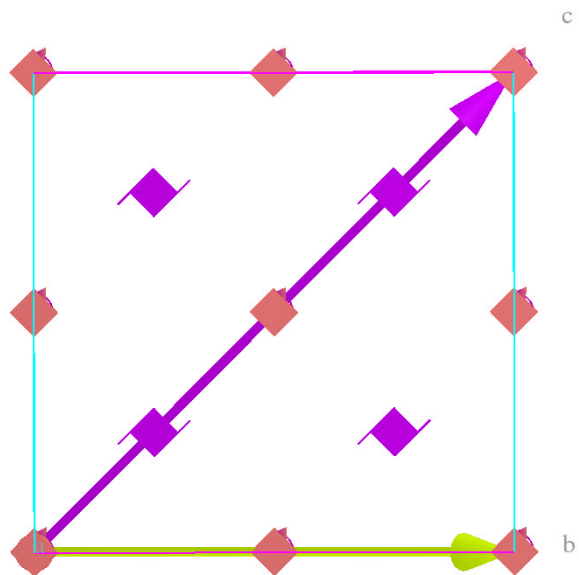


Fig. 20 Orthographic projection of Fig. 19 showing all  $90^\circ$  rotations and screws parallel to lattice vector  $a$  (vertical to paper plane), face diagonal  $c$  (in paper plane), and projected face diagonal  $b$ .

In Fig. 19 and Fig. 20 we can see how this works for the production of  $90^\circ$  screws. The orthographic projection in Fig. 20 can be directly compared with Fig. 18,  $\theta = 90^\circ$ . The fcc lattice has the side face centering translation  $T(b/2)$  as symmetry translation. The component of  $b/2$  in the plane perpendicular to  $a$  leads to the diagonal displacements of the rotation axis by  $c/4$ , the component of  $b/2$  parallel to  $a$  is  $a/2$ , it changes the dislocated rotation at  $c/4$  into a screw.

### 3.2.3 Explaining $180^\circ$ Screws

We skip details of the less difficult treatment of the  $180^\circ$ -screws, because here the axis displacements  $s$  in the rotation plane is simply half the displacement  $t$  in the rotation plane itself. In Fig. 21 we see the  $180^\circ$ -screws appear (compare Fig. 20) between neighboring  $90^\circ$  rotations (which are performed twice to produce  $180^\circ$  rotations before applying the translations).

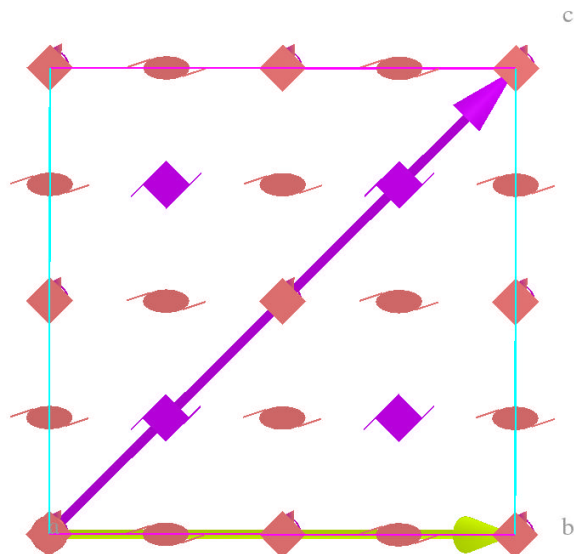


Fig. 21 Same as Fig. 20, but adding the  $180^\circ$ -screws generated by applying the face centering translations of the two vertical (to the paper plane) side faces.

### 3.2.4 Explaining $120^\circ$ Screws

Now we turn our attention to the  $120^\circ$ -screws. Fig. 22 shows in orthographic view all  $120^\circ$  rotation axis passing through an fcc cell, parallel to one selected space diagonal (this space diagonal is perpendicular to the face diagonal

vectors  $b$  and  $c$  of Fig. 19). In a simple cubic lattice only the axis  $R_{120}$  passing through the 8 cube vertexes are present, but the additional  $T(b/2)$  and  $T(c/2)$  translations in the plane of Fig. 22 generate according to Table 1 and Fig. 18 ( $s_{120}$ ) the additional twelve  $120^\circ$  rotation axis present in Fig. 22.

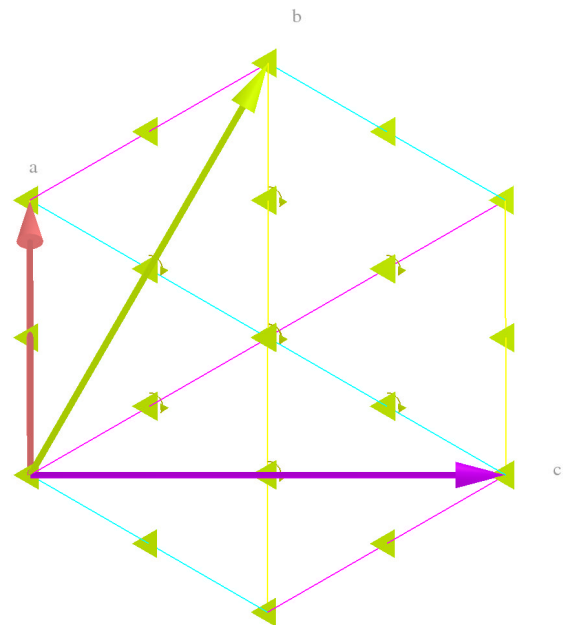


Fig. 22 All  $120^\circ$  rotations passing through one fcc lattice cell, in orthographic view along the selected (one of four) space diagonal axis. Vectors  $b, c$  in paper plane, vector  $a$  not.

Combining the translations  $T(a)$  and  $T(-a)$  with all the  $120^\circ$  Rotations of Fig. 22 produces all  $120^\circ$ -screws of Fig. 17. The component of  $a$  in the paper plane (plane of rotation) shifts the axis according to equation (6) and Table 1 (Fig. 18,  $s_{120}$ ) giving rise to a total of 12 screws. The translation component of  $a$  along the screw axis (perpendicular to the paper plane) points into the paper plane.

The same applies to the component of  $-a$  in the paper plane (only the sign of the resulting  $s_{120}$  changes), we therefore get the other 12 screws with opposite screw translations along the screw axis. The translation component of  $-a$  along the screw axis (perpendicular to the paper plane) points out of the paper plane.

We have thus accounted for all 24  $120^\circ$ -screws parallel to one space diagonal shown in Figs. 17 and 23. But in the cube all four space diagonals and all three edge vectors act as  $120^\circ$  rotation axis and as elementary lattice translations, respectively. Thus we get the total  $4 \cdot 24 = 96$

120°-screws.

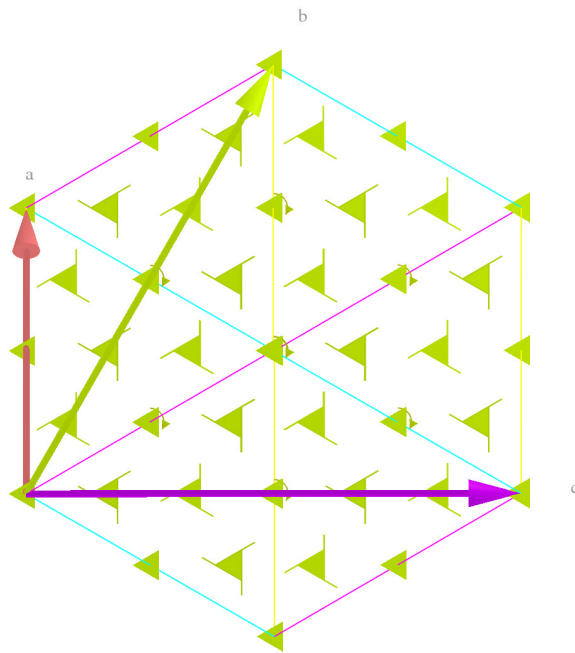


Fig. 23 All 120° rotations and screws (triangles with hooks) passing through one fcc lattice cell, in orthogonal view along the selected (one of four) space diagonal axis.

#### 4. CONCLUSIONS

We have given an extensive pictorial overview (using the SGV [7]) of the space group symmetry of the fcc gold lattice. A color version of this paper will be available from [17]. While reflections, glide reflections and rotations are rather elementary, the abundant presence of 192 screw axis passing through a single fcc cell for space group No. 225 (Hermann-Mauguin symbol:  $Fm\bar{3}m$ , geometric symbol:  $F43$ ) justified further explanation. Central to understanding the origin of screws is the law of combining rotations with lattice translations of section 3.2.1. Using the SGV we are often amazed by the intricate *beauty* of the combined display of symmetries (comp. Fig. 24). Yet looking e.g. at a gold ring, we have no perception for the tremendous immaterial form of beauty *hidden* inside.

We hope that the SGV will not only bring space group symmetry alive on the computer screen, and reveal its laws of geometry, but that it will also lead to a new appreciation of its beauty.

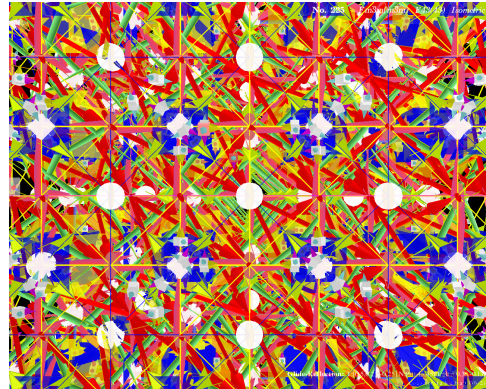


Fig. 24 Combined view symmetries of several gold (fcc) lattice cells.

#### 5. ACKNOWLEDGEMENTS

We gratefully acknowledge the fruitful exchange with David Hestenes, the repeated hospitality of the Cognitive Systems Group in Kiel, and the encouragement by Mois Arroyo to carry on with this project. E.H. thanks his family for its unwavering support and the Creator of all beauty: *Soli Deo Gloria*.

#### REFERENCES

1. D. Hestenes, J. Holt, *The Crystallographic Space Groups in Geometric Algebra*, Journal of Mathematical Physics, Vol. 48, No. 2 (2007).
2. T. Hahn (ed.), *International Tables of Crystallography*, Vol. A, 5th edition, Springer, 2005.
3. E. Hitzer, C. Perwass *Crystal Cells in Geometric Algebra*, in Proc. of ISAME, between University of Fukui (Japan)-Pukyong National University (Korea), 27 Nov. 2004, pp. 290-295 (2004). Online: <http://sinai.mech.fukui-u.ac.jp/gcj/publications/crystalc/crystalc.pdf>
4. C. Perwass, E. Hitzer *Interactive Visualization of Full Geometric Description of Crystal Space Groups*, in Proc. of ISAME, between University of Fukui (Japan), Pukyong National University (Korea) and University of Shanghai for Science and Tech. (China), 23-26 Nov. 2005. Online: <http://sinai.mech.fukui-u.ac.jp/gcj/publications/SGvisual/SGvisual.pdf>
5. E. Hitzer, C. Perwass *The Space Group Visualizer*, Proc. of ISAME, between University of Fukui (Japan), Pukyong National University (Korea) and University of Shanghai for Science and Technology

- (China), 26-29 Oct. 2006, pp. 172-181 (2006). Online: <http://sinai.mech.fukui-u.ac.jp/gcj/publications/TheSGV/TheSGV.pdf>
6. C. Perwass, *homepage of free open source software CLUcalc*, [www.clucalc.info](http://www.clucalc.info)
  7. C. Perwass, E. Hitzer, *homepage of the Space Group Visualizer project*, [www.spacegroup.info](http://www.spacegroup.info)
  8. *Gold, gold coin* entries of Wikipedia, <http://en.wikipedia.org/>
  9. D. Hestenes, *New Foundations for Classical Mechanics*, Kluwer Academic Publishers, Dordrecht, 1999.
  10. D. Hestenes, *Point Groups and Space Groups in Geometric Algebra*, in L. Dorst, C. Doran, J. Lasenby (eds.), *Applications of Geometric Algebra in Computer Science and Engineering*, Birkhaeuser, Boston, 2002, pp. 3-34. Online: <http://modelingnts.la.asu.edu/pdf/crystalsymmetry.pdf>
  11. E. Hitzer, C. Perwass, *Crystal Cell and Space Lattice Symmetries in Clifford Geometric Algebra*, in TE. Simos, G. Sihoyios, C. Tsitouras (eds.), ICNAAM 2005, Wiley-VCH, Weinheim, 2005, pp. 937-941. Online: <http://sinai.mech.fukui-u.ac.jp/gcj/publications/cellspacesym/cellspacesym.pdf>
  12. E. Hitzer, C. Perwass, *Full Geometric Description of All Symmetry Elements of Crystal Space Groups by the Suitable Choice of Only Three Vectors for Each Bravais Cell or Crystal Family*, in Proc. of ISAME 2005. Online: <http://sinai.mech.fukui-u.ac.jp/gcj/publications/SGtheory/SGtheory.pdf>
  13. E. Hitzer, C. Perwass, *Three Vector Generation of Crystal Space Groups in Geometric Algebra*, Bulletin of the Society for Science on Form, 21(1), pp. 55,56 (2006). Online: <http://sinai.mech.fukui-u.ac.jp/gcj/publications/tvgcsg/tvgcsg.pdf>
  14. E. Hitzer, C. Perwass, *Space Group Visualizer for Monoclinic Space Groups* Bull. Soc. Sci. on Form, 21(1), pp. 38,39 (2006). Online: <http://sinai.mech.fukui-u.ac.jp/gcj/publications/sgvmsg/sgvmsg.pdf>
  15. E. Hitzer, C. Perwass, *Crystallographic space groups: Representation and interactive visualization by geometric algebra*, submitted to Proceedings of the 26 ICGTMP, 29 June 2006, CUNY, USA.
  16. *Webelements periodic table* homepage: <http://www.webelements.com/>
  17. Publication download site of *Geometric*

*Algebra Group Fukui*, <http://sinai.mech.fukui-u.ac.jp/gcj/pubs.html>

18. D. Ichikawa, E. Hitzer, *Symmetry of Orthorhombic Materials and Interactive 3D Visualization with Geometric Algebra*, Proc. of ISAMPE 2007.
19. *Crystallographic Space Group Diagrams and Tables*, Hypertext Book, University of London, <http://img.chem.ucl.ac.uk/sgp/>

## APPENDIX

We now derive the solution of equation (5)

$$t-s = -R^{-1}sR \quad , \quad (A1)$$

using elementary *geometric algebra* [9,17], as introduced in the companion paper [18]. We therefore express the rotation operator (rotor)  $R$  like in equation (22) of [18] by two vectors  $a, b$  in the plane of rotation, subtending half the angle of rotation  $\theta/2$ :  $R=ab$ . Then equation (A1) becomes

$$t-s = -b^{-1}a^{-1}sab \quad . \quad (A2)$$

Successive geometric multiplication with  $b$  and  $a$  from the left gives

$$ab(t-s) = abt - abs = -s ab \quad . \quad (A3)$$

Adding  $bas$  on both sides and expanding the geometric product by  $ab = a \cdot b + a \wedge b$  gives

$$\begin{aligned} a \cdot bt + a \wedge bt \\ = a \cdot bs + a \wedge bs - sa \cdot b + sa \wedge b. \end{aligned} \quad (A4)$$

$a \cdot bs - sa \cdot b = 0$ , because  $a \cdot b$  is a scalar that commutes with  $s$ . The vectors  $a, b$  and  $s$  are all in the same plane, the bivector  $a \wedge b = |a||b|\mathbf{i} \sin \mathbf{q}/2$  anti-commutes therefore with  $s$ . So we get

$$2a \wedge bs = a \wedge bt + a \cdot bt. \quad (A5)$$

Division from the right with  $2a \wedge b$  yields

$$s = \frac{1}{2} \left( t + \frac{a \cdot b}{a \wedge b} t \right) = \frac{1}{2} \left( t + \frac{\cos \mathbf{q} / 2}{\mathbf{i} \sin \mathbf{q} / 2} t \right). \quad (A6)$$

The expression  $t = \mathbf{i}^{-1}t$  produces an anticlockwise 90° rotation of  $t$ . We thus arrive at solution (6), tabulated in Table 1.